NIH Public Access
Author Manuscript
Neuroimage. Author manuscript; available in PMC 2012 June 15.

Published in final edited form as:
Neuroimage. 2011 June 15; 56(4): 1908–1917. doi:10.1016/j.neuroimage.2011.03.043.

Dynamic imaging of ictal oscillations using non-invasive high-resolution EEG

Lin Yang[a,b], **Christopher Wilke**[a], **Benjamin Brinkmann**[c,d], **Gregory A. Worrell**[c,d], and **Bin He**[a,b,*]

[a]Department of Biomedical Engineering, University of Minnesota, Minneapolis, MN, USA

[b]Center for Neuroengineering, University of Minnesota, Minneapolis, MN, USA

[c]Department of Neurology, Mayo Clinic, Rochester, MN, USA

[d]Mayo Systems Electrophysiology Lab, Rochester, MN, USA

Abstract

Scalp electroencephalography (EEG) has been established as a major component of the pre-surgical evaluation for epilepsy surgery. However, its ability to localize seizure onset zones (SOZ) has been significantly restricted by its low spatial resolution and indirect correlation with underlying brain activities. Here we report a novel non-invasive dynamic seizure imaging (DSI) approach based upon high-density EEG recordings. This novel approach was particularly designed to image the dynamic changes of ictal rhythmic discharges that evolve through time, space and frequency. This method was evaluated in a group of 8 epilepsy patients and results were rigorously validated using intracranial EEG (iEEG) (n = 3) and surgical outcome (n = 7). The DSI localized the ictal activity in concordance with surgically resected zones and ictal iEEG recordings in the cohort of patients. The present promising results support the ability to precisely and accurately image dynamic seizure activity from non-invasive measurements. The successful establishment of such a non-invasive seizure imaging modality for surgical evaluation will have a significant impact in the management of medically intractable epilepsy.

Keywords

High-resolution EEG; Dynamic seizure imaging; Pre-surgical planning

Introduction

Epilepsy is one of the most common neurologic disorders, affecting an estimated 50 million people worldwide. Antiepileptic drugs form the initial line of treatment for patients suffering from epileptic seizures and a majority of treated individuals will experience cessation or significant reductions in the frequency of seizures. While medical therapy is successful in many patients, a significant minority, some 30% of those suffering from epilepsy, will continue to have uncontrolled seizures despite optimal medical management. For this subset of refractory patients, surgical resection of the epileptogenic cortex is one of the remaining treatment modalities (Kuzniecky and Devinsky, 2007).

© 2011 Elsevier Inc. All rights reserved.

*Corresponding author at: University of Minnesota, Department of Biomedical Engineering, 7–105 Hasselmo Hall, 312 Church Street, Minneapolis, MN 55455, USA. binhe@umn.edu.

NIH-PA Author Manuscript
NIH-PA Author Manuscript
NIH-PA Author Manuscript

NIH-PA Author Manuscript

NIH-PA Author Manuscript

NIH-PA Author Manuscript

For decades, scalp EEG has been considered one of the important diagnostic procedures to identify the SOZ that must be delineated in order to determine if the patient is a candidate for surgical resection. Scalp EEG has the advantages of non-invasiveness, low risks and low cost compared to intracranial EEG (iEEG), which is currently the gold standard for localizing seizure activity (Carmichael et al., 2010; Rosenow and Luders 2001) or the eloquent functional brain (Towle et al., 2008). At the same time, scalp EEG shares the excellent temporal resolution of iEEG and is the only non-invasive tool capable of dynamically measuring the onset and generalization of seizure activity. Other imaging techniques with minimal invasiveness (Blumenfeld et al., 2009; Knowlton et al., 2008; Laufs and Duncan, 2007; Tyvaert et al., 2008; Vitikainen et al., 2009) such as single photon emission computerized tomography (SPECT) and functional magnetic resonance imaging (fMRI) have also been proved useful to assist in the delineation of epileptogenic brain. Yet their lack of temporal resolution restricts the ability to separate the primary seizure focus from propagation areas. Nevertheless, scalp EEG has yet to be considered a precise imaging tool for the identification of SOZ. Its localization ability is restricted by intrinsic limitations, including low spatial sampling rate (typically 19–32 electrodes rendering ~5 cm inter-electrode distance) and indirect correlation with underlying neural generators due to volume conduction effect. Simple visual inspection of EEG waveforms, which is commonly used in clinical practice, remains inadequate for the precise delineation of the SOZ in the absence of structural abnormalities observed on anatomic imaging studies.

Recent technical development of source imaging techniques (Assaf and Ebersole, 1997; Plummer et al., 2008) suggest that the traditional visual interpretation of EEG waveforms does not take full advantage of the intrinsic linkage between scalp potentials and their underlying neural generators. Beyond the capability of scalp mapping, it has been shown that EEG recordings along with the assistance of source imaging techniques allow improved localization of scalp EEG events onto the underlying brain structures. Particularly, with the recent development of high-resolution recording techniques, such as densearray EEG (Holmes et al., 2010; Koessler et al., 2010; Lantz et al., 2003) and magnetoencephalography (MEG) (Baumgartner and Pataraia, 2006), EEG/MEG source imaging techniques have been increasingly explored as a pre-surgical imaging tool for the identification of SOZ. But many of these EEG/MEG studies have focused on source imaging of interictal spikes and short epileptiform discharges (Knowlton et al., 2008; Knowlton et al., 2009; Lantz et al., 2003; Minassian et al., 1999) as opposed to ictal periods, although the precise correlation of the cortical distribution of these events with the clinical SOZ remains unclear (Marsh et al., 2010). A reliable recording of seizure data, which requires prolonged monitoring of patients for 2 or more days and the development of methodologies to image dynamic ictal process, still remain as two principal challenges for seizure imaging.

In this context, the present study aimed to develop a high resolution seizure imaging protocol for potential application in presurgical planning of the epilepsy treatment. We proposed a 76-electrode EEG monitoring system. In a cohort of 8 patients, this densearray EEG system successfully recorded EEG over the course of 5.5 ± 3.2 days and was able to capture each clinical event (1–4 seizures per patient). We have also developed a novel DSI technique (Fig. 1) that is particularly well-suited for spatiotemporal imaging of ictal rhythmic discharges. The DSI technique identified ictal activity in good correlation with iEEG and surgical outcomes. Such a seizure imaging tool characterizing high resolution in both time and space could significantly enhance pre-operative planning and have a major impact in the management of intractable epilepsy.

NIH-PA Author Manuscript

NIH-PA Author Manuscript

NIH-PA Author Manuscript

Materials and methods

Patients and data acquisition

We studied 8 adult patients (4 male, and 4 female, ages 40 ± 11.6) with medically intractable epilepsy requiring a resective surgery or subsequent exploration with iEEG. The study was approved by the Institutional Review Boards of the University of Minnesota (Minneapolis, MN) and Mayo Clinic (Rochester, MN) and all patients gave informed consent.

Each patient underwent pre-surgical evaluation, including a highresolution 3T or 1.5T MRI scan (n = 8), iEEG recording (n = 3), and SPECT scans (n = 1). In addition to the regular procedures, each patient underwent high-resolution video EEG monitoring (5.5 ± 3.2 days) using 76 individual electrodes glued over the scalp according to a 10–10 montage. The EEG recordings were referenced to CPz, passed through a 1–70 Hz band pass filter, and sampled at 500 Hz. Following the acquisition of the data, the recordings were visually reviewed and a total of 20 seizures (range 1–4 per patient) were identified. The seizure onset time of each seizure was marked by trained clinical epileptologists. Seven of the patients had surgical resection of the epileptogenic foci and all became seizure free during clinical follow-up 1 year post-operatively. All of these patients had an additional MRI scan 3–4 months post-operatively. The other patient (patient 4) underwent iEEG and SPECT scans as part of the presurgical evaluation. Detailed clinical information of the patients is summarized in Table 1.

Data analysis and seizure source imaging

The DSI method aims to acquire dynamic imaging of ictal rhythmic activity. In order to do this, it is necessary that continuous synchronized rhythmic discharges be observed following the seizure onset. As such, of the 20 seizures recorded we discarded 3 due either to the presence of significant moving artifacts in a large number of electrodes or the absence of continuous rhythmic activity around seizure onset time. We segmented ictal epochs ~30 seconds before and following the seizure onsets of the other 17 seizures. The window length for each epoch was varied to avoid big moving artifact, and also to include a period of background signal before seizure onset and a period of highly synchronous seizure activity following the onset. The period of secondary generalization was not included. In each patient, ictal epochs presenting the same rhythmic discharges were concatenated.

The DSI procedure consists of: (1) disentanglement of seizure components from ictal EEG data, (2) localization of neural generators of seizure components, and (3) recombination of all the seizure components in 3-dimensional (3D) brain source space to form spatiotemporal imaging of the seizure activity. This method was designed particularly for the imaging of continuous rhythmic activity. The framework of the DSI method is illustrated in Fig. 1.

In the EEG forward modeling, spatiotemporal EEG signal Y can be related with underlying brain activity S through a linear system:

$$\mathrm{Y} = \mathrm{L}\,\mathrm{S} + \mathrm{B} \tag{1}$$

where $\mathrm{Y}\left(\vec{r}, t\right)$ is an $n \times t$ signal matrix (n is the number of electrodes and t is the number of time points), $\mathrm{S}\left(\vec{r}, t\right)$ is an $m \times t$ source matrix (m is the dimension of source space) and B is a $n \times t$ noise matrix. L is an $n \times m$ lead field matrix that can be calculated based on the boundary element method (BEM) (Fuchs et al., 1998; Hamalainen and Sarvas 1989; He et al., 1987). In the BEM model, the head volume conductor was separated into three conductive layers, the brain, the skull and the skin with conductivity of 0.33 S/m, 0.0165 S/m and 0.33 S/m, respectively (Lai et al., 2005; Oostendorp et al., 2002; Zhang et al., 2006).

NIH-PA Author Manuscript

NIH-PA Author Manuscript

NIH-PA Author Manuscript

A 3D distributed source model was used to model the brain source distribution that consists of around ten thousand equivalent current dipoles with unconstrained orientations evenly positioned within the 3D brain volume. Standard electrode positions were used for the calculation.

Ictal EEG measures seizure rhythmic discharges that evolve through time, space and frequency (Nam et al., 2002; Patel et al., 2008), superposed with measurement noise, moving artifacts and other background brain oscillations (Jung et al., 2000; Urrestarazu et al., 2004). To analyze such complicated signal, independent component analysis (ICA) was used to decompose each ictal EEG into a series of temporally independent and spatially fixed components as follows (Delorme and Makeig, 2004):

$$Y = W Q T = \sum_{i=1}^{Nc} w_i Q_i T_i \tag{2}$$

where N_c is the number of ICs, $\mathbf{Q}_i$ (ith column of the matrix $\mathbf{Q}_{n \times NC}$)is the spatial map of the ith IC, $\mathbf{T}_i$(ith row of matrix $\mathbf{T}_{Nc \times t}$) is the time course of the ith IC, and $\mathbf{W}$ is a diagonal weighting matrix. Assuming N_S out of the N_c ICs are associated with seizure activities (details of component selection will be discussed later), the scalp measurement generated by ictal Ns conditions becomes $Y = W Q T = \sum_{i=1}^{Ns} w_i Q_i T_i$

Given the forward modeling of lead field matrix, spatiotemporal brain sources can be estimated from the EEG measurements by solving an inverse problem as follows (Pascual-Marqui et al., 1994):

$$\widehat{S} = L^{-1} Y \tag{3}$$

where $\mathbf{L}^{-1}$ is the inverse of lead field matrix. Substituting Eqs. (2) into (3), the spatiotemporal estimation can be rewritten as:

$$\widehat{S} = L^{-1} \sum_{i=1}^{Ns} w_i Q_i T_i = \sum_{i=1}^{Ns} \left[L^{-1} Q_i \right] w_i T_i = \sum_{i=1}^{Ns} \widehat{S}_i w_i T_i \tag{4}$$

where $\widehat{S}_i = L^{-1} Q_i$ is the source distribution of the ith IC, and $\sum_{i=1}^{Ns} \widehat{S}_i w_i T_i$ is the linear combination of seizure components in the in source space, which can be seen as an inverse process of ICA. Here, we used a well adopted algorithm known as Low Resolution Electromagnetic Tomography (LORETA) (Pascual-Marqui et al., 1994) to estimate $\mathbf{S}_i$ of each seizure component. However, other EEG/MEG spatial imaging algorithms such as minimum norm, weighted minimum norm, or fMRI-weighted minimum norm (Yang et al., 2010) can be easily incorporated by just changing the inverse operator $\mathbf{L}^{-1}$. Given the reconstructed dynamic source signal $\hat{\mathbf{S}}$, spatial distribution at time instant t' can be reconstructed and visualized as:

$$\widehat{S}\left(\vec{r}, t'\right) = \widehat{S}\left(\vec{r}, t = t'\right) \tag{5}$$

While t' is the seizure onset time instant, the $\widehat{S}\left(\vec{r}, t'\right)$ quantifies the source distribution of the SOZ. Similarly, the time-variant propagation of seizure activity over the prolonged ictal period can also be visualized during time window after the seizure onset.

NIH-PA Author Manuscript

NIH-PA Author Manuscript

NIH-PA Author Manuscript

Component selection

Seizure activities are characterized by abnormal synchrony of neuronal rhythmic discharges. Time–frequency evolution pattern of ictal rhythmic discharges is observable in raw EEG recordings and also in ICs related with ictal conditions (Nam et al., 2002; Patel et al., 2008). As such, the time–frequency similarity between the two signals was used in this study for the selection of seizure components.

In each seizure recording, visual inspection was first performed to remove those ICs showing continuous activity or transit spikes (e.g., in IC time courses or spectrograms) not correlated with seizure conditions, such as the eye movement components which showed IC spatial maps with frontal eye activity (Jung et al., 2000; Urrestarazu et al., 2004) and moving artifactual components which showed strong power invariant across all the frequency bands and/or with spatial maps dominated by noise (Hansen 1990). The noise-deducted EEG was then reconstructed. We picked the electrodes identified by epileptologists that showed ictal rhythmic discharges and calculated the mean time–frequency representation (TFR) of EEG recorded by these electrodes (EEG-TFR) using short time Fourier transformation (sliding window size 500 time points, 50% overlapping). We then computed a TFR for each IC (including all the ICs derived from ICA). Correlations between each IC-TFR and EEG-TFR were calculated. Statistical significance of the correlation between EEG-TFR and each IC-TFR was quantified by a nonparametric statistical test technique using a surrogate method (Palus and Hoyer, 1998; Theiler et al., 1992). In the test, surrogate datasets were created from EEG signal and each IC time course so that their mutual correlations were not preserved. For each IC, new correlations between EEG-TFRs and IC-TFRs were computed from surrogated datasets and a distribution of correlation values was obtained. From the distribution, statistical significance of an IC-EEG-correlation can be decided and we selected those components exceeding a threshold of $p=0.1$ as seizure components for further source analysis. The threshold of p value may change slightly for each patient. Visual inspections were used to assist the selection of seizure components. Other component selection methods such as clustering techniques can be readily incorporated into the framework of DSI for specific application of different studies.

Validation using iEEG and surgical outcomes

Given the estimated spatiotemporal source signal, the SOZ was defined as the source distribution at onset time instant. We first use the surgically resected region as a reference to quantitatively evaluate the performance of the SOZ localization. In each patient who underwent resective surgery followed by a post-operative MRI scan, we segmented the surgically resected zone from the post-operative MRI and coregistered the resected area to the pre-operative MRI. For each seizure, the spatial overlapping between the estimated SOZ (60% threshold as shown in all the figures) and the surgically resected zone was calculated.

We then used the receiver operating characteristic (ROC) curve (Grova et al., 2006) to quantify the consistency of the estimated SOZ source distribution with surgically resected zone. The ROC curve studies the trade-off between sensitivity and specificity of SOZ source detection at different thresholds ranging from 0 to 100%. The area under the ROC curve (AUC) is an index to assess the localization accuracy. A larger value of AUC in the range of [0,1] means better source detection ability. We lastly used localization error, which was calculated as the 3D distance between the maximal estimated point and the boundary of the surgically resected region, to assess the performance of SOZ localization. If the maximal point was localized within the resected zone, we defined the distance as 0 mm. For patient 4 who did not undergo surgery, SPECT foci identified through Subtraction Ictal SPECT (SISCOM) analysis (Brinkmann et al., 2000) were used to compare with the estimated SOZ and to evaluate the performance in terms of volume overlapping and localization error.

NIH-PA Author Manuscript

NIH-PA Author Manuscript

NIH-PA Author Manuscript

Intracranial depth electrodes, stripes and grids were implanted in patients 2–4. The iEEG recordings of these three patients were visually reviewed and the electrodes involved in the seizure onset were identified by epileptologists (see Table 1 for clinical information). The 3 patients all underwent CT scanning while the electrodes were implanted. The positions of the intracranial electrodes were determined from the CT images and co-registered to the pre-operative MRI. The SOZs identified using iEEG were used to qualitatively evaluate the performance of the DSI method.

Imaging seizure activity by directly solving inverse problem instant by instant is a straightforward method to estimate the source distribution during ictal period (Holmes et al., 2010). We thus perform source imaging using the LORETA algorithm at seizure onset time of raw EEG. The performance of SOZ localization was evaluated and compared with the DSI method using three measures: volume overlapping, AUC value and localization error as described above. Because of the low signal-to-noise ratio (SNR) of the raw EEG signal at the seizure onset, LORETA may achieve better source localization when more brain tissue is involved after the onset of seizure. As such, we performed LORETA source imaging on a segment of the raw EEG signal 50 ms before and following the seizure onset. For each seizure, the best source localization within the 100 ms window was used to assess the performance of source localization.

Results

Spatial and temporal representations of ictal rhythms

Using ICA and component selection, multiple ICs can be identified from each seizure to represent ictal activity. 1 Patient presented with frontal lobe epilepsy. Using ICA, two components were identified from one seizure (Fig. 2a) showing increased neural synchrony initiated with fast rhythmic activity at the seizure onset that later progressed to an alpha frequency discharge. This time–frequency evolution pattern of the ictal rhythmic discharges can be visualized in both IC time courses and their TFRs, and was consistent with independent observation reported by clinical epileptologists. The scalp map showed left frontal focus of the seizure components with some spread to the temporal lobe in the 2nd component. The three seizures recorded in this patient presented similar EEG rhythmic discharges. One example component identified from another seizure of the patient (Fig. 2b) showed similar rhythmic discharges at the seizure onset. Its scalp map further localized this seizure component to the left frontal electrodes.

Patients 2–8 all presented with temporal lobe foci in the left or right hemispheres. In each of the 14 seizures analyzed in these 7 patients, multiple ICs were identified as seizure components (seeFig. 2c for an IC example in each patient). Three patterns of ictal rhythmic discharges were observed from IC time courses and TFRs. At seizure onset, one pattern (patients 2, 3 and 5) showed initial delta frequency discharges that later progressed to theta frequency, another pattern (patients 6, 7 and 8) showed initial theta discharges, and the third pattern (patient 4) presented alpha discharges.

Dynamic spatiotemporal imaging and SOZ localization

The SOZ of patient 1 was reconstructed in a 3D brain model (Fig. 3a, 60% threshold, yellow to orange color bar). A surgical excision was performed from the anterior left frontal lobe of this patient. Upon visual inspection, a significant portion of the estimated SOZ was localized to the epileptogenic focus resected in the left frontal lobe (Fig. 3a, green voxels). Quantitatively, the brain voxel with maximal estimated source power was located within the surgically resected zone. The patient was rendered seizure free following surgery, which

NIH-PA Author Manuscript

NIH-PA Author Manuscript

NIH-PA Author Manuscript

suggests that the estimated SOZ was co-localized with the epileptogenic zone removed in the surgery.

The SOZs of the other 7 patients (patients 2–8) were localized using DSI to the left or right temporal lobe. Among these patients, three (patients 2–4) were implanted with intracranial electrodes (Figs. 3b–d, spherical dots). Independent visual interpretation of the iEEG reported by clinical epileptologists (Table 1) identified seizure onsets in the temporal lobe electrodes (Figs. 3b–d, red dots). It can be observed that the DSI localization in the three patients (Figs. 3b–d) was consistent with or in adjacent to the clinical gold standard iEEG. Among the 7 patients, six (patients 2, 3, 5–8) underwent resective surgery and were rendered seizure-free after 1 year follow-up. In each of the 13 seizures analyzed in this group, significant overlap was observed between the estimated SOZ and surgical resected volume. The maximal estimated points were localized within the resected regions in 11/13 seizures, and within 10 mm distance to the margins of resected regions in the remaining 2/13 seizures. Patient 4, who did not undergo resective surgery, had SPECT scans as part of the presurgical evaluation. SISCOM analysis suggested several adjacent foci of ictal hyperperfusion in the right temporal lobe (Fig. 3d, green voxels), which may also serve as an evidence of right temporal lobe seizure. The DSI analysis in this patient returned right temporal foci at seizure onset, which was co-localized with iEEG results (Fig. 3d) and had a 10.9-mm distance to the boundary of SPECT foci. The SOZs localized using DSI of all the 17 seizures were summarized in Fig. 6. In the majority of the seizures, the estimated SOZs are located within the epileptogenic lobe, whereas in the seizure of patient 7 and the seizure 2 of patient 6, small areas of activation were seen outside of the epileptogenic lobe, which were false positives of source detection.

In all the 17 seizures analyzed, the DSI method achieved colocalization in 14 seizures and 0.99±0.16-cm localization error in the remaining 3 seizures. Estimation of two seizures showed false positive outside the epileptogenic lobe. The performance of this approach achieved better results than directly applying source imaging of the raw EEG data instant-by-instant, which had 2.8 ±0.98-cm localization error. While DSI estimated distributed source activity, volume overlap may be a better measure to evaluate the performance of imaging the location and extent of SOZ. At a 60% threshold, the DSI identified SOZs with significantly higher volume overlap with the resected zones or SPECT imaging (Fig. 4a). We further assessed the localization accuracy through the ROC curve (Grova et al., 2006). The AUC measure (Grova et al., 2006)(Fig. 4b) was used as an index to evaluate the localization accuracy, which suggested that the DSI reconstructed the source distribution at seizure onset with greater precision.

In addition to determining the SOZ, DSI reconstructs propagated activity after seizure onset. Shown in Fig. 5, from the estimated spatiotemporal source activity $\hat{S}(t)$, time-varying source power in each brain voxel was calculated as the spectral power within the predominant frequency band of ictal rhythm during a 1-s time window. The source power distribution over the ictal period suggested the propagation of seizure activity from a focal location to extended regions ipsilaterally or contralaterally. As the source power was calculated in a short time window, some spread of the source distribution to adjacent cortex, such as the area of activation in frontal cortex of patient 3 and 7, was observed in early instants (Fig. 5). Also, source time–frequency features can be reconstructed in the 3D source space. Fig. 3 (right panels) displays TFRs of the SOZ tissue and shows the time–frequency features of each seizure. Although we use 1-s time window here, movies of seizure source activity can be shown in a much finer time scale.

NIH-PA Author Manuscript

NIH-PA Author Manuscript

NIH-PA Author Manuscript

Discussion

In this study, we have developed a high-resolution EEG monitoring and dynamic source imaging approach for the pre-surgical localization of seizure onset zones and seizure propagation patterns in epilepsy patients. We tested the method in a cohort of 8 patients, imaging the ictal rhythmic activity in good correlation with other clinical imaging or diagnostic evidence. The results demonstrated the feasibility and usefulness of a novel 76-channel EEG ictal recording and DSI procedure, which could represent a significant advancement for non-invasive pre-surgical planning of patients with epilepsy.

High-resolution ictal recording

Over the past thirty years, numerous studies have been conducted to support an advanced high-resolution form of non-invasive electromagnetic recording (e.g. dense-array EEG (Gevins, 1993) and MEG (Hämäläinen et al., 1993)). Theoretical and experimental studies suggested recordings from approximately 100 scalp sites for a good spatial sampling rate and a stable spatial representation (Spitzer et al., 1989; Srinivasan et al., 1996). In the clinical realm, while standard EEG monitoring still uses conventional 19-to-32-electrode montages, recent adoption of high-resolution EEG/MEG for the pre-surgical localization of partial epilepsy has increased in popularity. One EEG study (Lantz et al., 2003) revealed in a case of inter-ictal discharges that the localization accuracy can be significantly improved by increasing the number of EEG electrodes from 31 to 63, yet only slightly improved by increasing the number from 63 to 123. Studies conducted in various epilepsy centers have produced good source detection rates in a number of patients (Assaf et al., 2004; Baumgartner and Pataraia, 2006; Knowlton et al., 2008; Pataraia et al., 2004; Stefan et al., 2003; Wheless et al., 1999; Michel et al., 2004; Holmes et al., 2010). According to these previous studies, increasing the channel number to 76, as in our study, significantly provides more spatial detail for the localization of epileptic sources. Most of the clinical application of high-resolution EEG and MEG has been restricted to imaging of inter-ictal spikes. Studies have demonstrated good correlation between sources of inter-ictal spike and epileptogenic regions (Michel et al., 2004; Knowlton et al., 2008). Intracranial studies further suggested that the onset of inter-ictal spike localizes the seizure onset zone better than the peak of spikes when propagation happens (Ray et al., 2007). However, it is also well known that the irritative zone defined by inter-ictal spikes does not reliably determine the minimum region of brain tissue that must be resected in order to render the patient seizure free (Marsh et al., 2010). The availability of reliable seizure imaging would provide highly desirable information with regard to the underlying seizure sources which would directly define the SOZ that must be resected.

One technical limitation of seizure imaging lies in the recording environment where the patients are required to stay motionless in order to obtain high-quality signals. This is especially true for MEG recordings. Such a requirement adds a level of difficulty for prolonged clinical monitoring which ordinarily lasts for 2–3 days or longer in patients with infrequent seizures. In our study, the clinical data presented was recorded over 5.5 ±3.2 days allowing for the acquisition of 1–4 seizures per patient. The 76-channel montage successfully captured each clinic event in the examined cohort of patients, producing a yield rate of 100%. The increased implementation time could be a potential disadvantage of high-density EEG. However, it only required an average of 60 min to mount the 76 electrodes by two experienced medical staff, compared to 30 min using a standard 32-channel clinical EEG. Recent studies have reported a fast-capping EEG technique for which the preparation time can be as short as 15 min (Holmes et al., 2010). Such a technique however is limited by relatively shorter recording time due to the fact that patients usually cannot comfortably wear the device for more than 2 to 3 days (Holmes et al., 2010). The 76-channel recording protocol, on the other hand, was identical with the conventional clinical EEG whose

NIH-PA Author Manuscript

NIH-PA Author Manuscript

NIH-PA Author Manuscript

feasibility of long-term monitoring has been demonstrated over several decades' worth of clinical practice. The 76-channel EEG can be a feasible clinical EEG monitoring tool, which requires minimal increase of costs (e.g., preparation time, additional electrodes, and additional amplifiers) but provides significantly improved spatial resolution for the localization of the SOZ.

Dynamic imaging of seizure activity

Another difficulty for seizure imaging lies in the development of methodologies to reconstruct dynamic ictal rhythmic discharges from continuous EEG data. Fitting single or multiple dipoles in the time domain or in the frequency domain (Assaf and Ebersole 1997; Assaf et al., 2003; Boon et al., 2002; Eliashiv et al., 2002; Merlet and Gotman, 2001; Lantz et al., 1999) of the early activation of ictal rhythms has been demonstrated as useful in providing sublobar prediction of seizure origin in temporal lobe seizures and extra-temporal lobe seizures. Such methods need prior information such as the number of dipoles or the positions of dipoles which cannot be easily gained from EEG signal alone. Sub-space scanning methods, such as MUSIC (Mosher et al., 1992; Beniczky et al., 2006) and FINE (Ding et al., 2007) also provide the ability to reconstruct temporal dynamics of seizure sources, and, in conjunction with connectivity analysis, were able to discriminate the seizure onset and propagation (Ding et al., 2007). In these situations, however, the limited number of equivalent dipoles (as discrete sources) may not be an appropriate representation of the distributed brain activity involved in seizures. Assuming a distributed nature of seizure activity, a straightforward method entails conducting source imaging instant by instant to find neural generators responsible for each millisecond or for each short time window (Holmes et al., 2010; Worrell et al., 2000). Due to the significant amount of information in ictal EEG, such a process may require solving thousands of inverse problems in order to achieve several-second-long source imaging. Also, noise and artifactual signals at the time of seizure onset adds a level of complexity for the disentanglement of seizure source (Jung et al., 2000; Urrestarazu et al., 2004; Worrell et al., 2000). A previous study (Lantz, et al., 2001) improved the analysis of ictal EEG by segmenting ictal period into "microstates" and localized the seizure onset by searching for dominant "microstates" during the early phase. Such a method provides a way to decrease the complexity of seizure data. In the present study, our method offers a quantitative means to identify and image seizure sources in a highly efficient way.

In the present study, we developed a dynamic source imaging technique that is particularly suited for imaging of oscillatory activity such as seizure expanding from several seconds to several minutes. This dynamic spatiotemporal imaging approach is achieved by a decomposition–recombination process, where the decomposition was taken in the sensor space and the recombination is taken in the source space. By using such a process, regardless of the length of continuous seizure data, only a limited number (equal to the number of selected seizure components) of inverse problems are needed to be solved. Additionally, the separation of ictal components from artifacts, noise and other background brain oscillations largely enhances the source analysis. This approach can be also seen as a time–space-separated process. The data-driven ICA analysis decomposes the signal into several spatially fixed but temporally dynamic components. In the time domain, the time–frequency evolution represented in the time course assisted the selection of the seizure components. This step of component selection allows for the extraction and imaging of certain rhythmic modulation (e.g., delta rhythm that later progressed to theta rhythm presented in a large portion of our patients), and thus is well suited to study the time-varying ictal rhythmic activity.

Epilepsy patients with partial seizure may develop secondary generalization, during which complicated activity and propagation can be involved. Recent evidence of SPECT recording

NIH-PA Author Manuscript

NIH-PA Author Manuscript

NIH-PA Author Manuscript

(Blumenfeld et al., 2009) and intracranial recording (Schindler et al., 2007) suggests that "generalized" seizures may not be truly generalized but affect certain cortical and subcortical structures. The investigation of these brain structures involved in generalized seizure may help to develop improved treatment for this most dangerous seizure type. In the present study, three patients presented seizures with secondary generalization after a period of focal features. The period of generalization was not included for the analysis because the seizure onset and early activation are of most clinical importance for the treatment of partial epilepsy. But the propagation pattern of generalized seizure would be of importance for our future investigation.

Localization of seizure onset zone

The diagnostic practice of EEG in epilepsy treatment has remained relatively unchanged for the past several decades (Gevins 1993; Kuzniecky and Devinsky 2007; Rosenow and Luders, 2001). Visual interpretation of EEG waveforms provided a coarse approximation of the SOZ, whereas a more precise localization is determined by iEEG or the presence of an epileptogenic MRI lesion. The DSI results indicate that the SOZs can be successfully localized by high-resolution EEG imaging in a cohort of 8 patients. We analyzed 17 seizures, 3 with frontal lobe focus and the remaining 14 with temporal lobe focus. In each of the 17 seizures, the location and extension of the estimated SOZ is in good correlation with the epileptogenic zone resected in surgery or defined by iEEG/SPECT imaging methods. The maximal localization error we derived was less than 11 mm. In the majority of the seizures analyzed, the estimated SOZs are located within or proximal to the epileptogenic lobe, whereas in the other two seizures small areas of activation were seen outside of the epileptogenic lobe. These false positive areas of activation outside of the epileptogenic brain could represent a secondary source, which was activated very early in the ictal process, but was not a primary source that initiated the seizure activity (Ding et al., 2007; Franaszczuk et al., 1994). For example, patient 6, though seizure free still experienced intermittent auras following the resective surgery. This ILAE-2 outcome according to International League Against Epilepsy (ILAE) suggested that it is possible some parts of the brain (e.g., false positives imaged using EEG in SZ2 of this patient) other than the resected region may be still capable of generating seizure-like activity. Also, this false positive can be explained by the rapid spread of the seizure activity that, when detected by EEG, has already been propagated.

As has been tested in the patient cohort presented here, our results suggest that beyond the traditional role of scalp EEG in epilepsy treatment, high-resolution EEG can be used as a pre-surgical imaging tool which provides additional information about the precise location and extent of the SOZ. Currently, iEEG still remains the golden standard for determining the SOZ. However, it is also true that iEEG brings added costs and risks to the management of epilepsy. iEEG grids or electrodes are only positioned at the most suspicious regions, which are decided by prior knowledge gained from scalp EEG or other clinical information. In our study, high-resolution EEG in conjunction with DSI, which is less expensive and contains far less risk to the patient, showed promise for assisting in the placement of iEEG electrodes or potentially mitigate or supplant the use of invasive EEG recordings in situations where SOZ localization is ambiguous through conventional clinical methods. In patients with evidence of a lesion on pre-operative MRI, the high-resolution EEG imaging can also be a useful tool to improve lesion detection, and therefore enhances the successful rate of epilepsy surgery.

Although the analysis in this study is based on 76-channel EEG recording, the DSI method can be also used to analyze low-density EEG data, or other dense-array EEG data (e.g., 128-channel fast-capping EEG system), or continuous MEG data. While the DSI technique was

NIH-PA Author Manuscript

NIH-PA Author Manuscript

NIH-PA Author Manuscript

validated in epilepsy patients in the present study, the imaging principle and algorithm of DSI may be used to image rhythmic activity of healthy or diseased brains.

Acknowledgments

This work was supported by NIH RO1 EB007920, RO1 EB006433 and NSF CBET-0933067 (B.H.). The authors would like to thank Cindy Nelson for technical assistance in data collection, and Dr. Gang Wang for assistance in data analysis.

References

Assaf BA, Ebersole JS. Continuous source imaging of scalp ictal rhythms in temporal lobe epilepsy. Epilepsia. 1997; 38(10):1114–1123. [PubMed: 9579958]

Assaf BA, Karkar KM, Laxer KD, Garcia PA, Austin EJ, Barbaro NM, Aminoff MJ. Ictal magnetoencephalography in temporal and extratemporal lobe epilepsy. Epilepsia. 2003; 44(10): 1320–1327. [PubMed: 14510826]

Assaf BA, Karkar KM, Laxer KD, Garcia PA, Austin EJ, Barbaro NM, Aminoff MJ. Magnetoencephalography source localization and surgical outcome in temporal lobe epilepsy. Clin. Neurophysiol. 2004; 115(9):2066–2076. [PubMed: 15294209]

Baumgartner C, Pataraia E. Revisiting the role of magnetoencephalography in epilepsy. Curr. Opin. Neurol. 2006; 19(2):181–186. [PubMed: 16538094]

Beniczky S, Oturai PS, Alving J, Sabers A, Herning M, Fabricius M. Source analysis of epileptic discharges using multiple signal classification analysis. Neuroreport. 2006; 17(12):1283. [PubMed: 16951570]

Blumenfeld H, Varghese G, Purcaro M, Motelow J, Enev M, McNally K, Levin A, Hirsch L, Tikofsky R, Zubal I. Cortical and subcortical networks in human secondarily generalized tonic–clonic seizures. Brain. 2009; 132(4):999. [PubMed: 19339252]

Boon P, D'Havé M, Vanrumste B, Van Hoey G, Vonck K, Van Walleghem P, Caemaert J, Achten E, De Reuck J. Ictal source localization in presurgical patients with refractory epilepsy. J. Clin. Neurophysiol. 2002; 19(5):461. [PubMed: 12477991]

Brinkmann BH, O'Brien TJ, Mullan BP, O'Connor MK, Robb RA, So EL. Subtraction ictal SPECT coregistered to MRI for seizure focus localization in partial epilepsy. Mayo Clin. Proc. 2000; 75:615–624. [PubMed: 10852423]

Carmichael DW, Thornton JS, Rodionov R, Thornton R, McEvoy AW, Ordidge RJ, Allen PJ, Lemieux L. Feasibility of simultaneous intracranial EEG-fMRI in humans: a safety study. Neuroimage. 2010; 49(1):379–390. [PubMed: 19651221]

Delorme A, Makeig S. EEGLAB: an open source toolbox for analysis of singletrial EEG dynamics including independent component analysis. J. Neurosci. Methods. 2004; 134(1):9–21. [PubMed: 15102499]

Ding L, Worrell GA, Lagerlund TD, He B. Ictal source analysis: localization and imaging of causal interactions in humans. Neuroimage. 2007; 34(2):575–586. [PubMed: 17112748]

Eliashiv D, Elsas S, Squires K, Fried I, Engel J Jr. Ictal magnetic source imaging as a localizing tool in partial epilepsy. Neurology. 2002; 59(10):1600–1610. [PubMed: 12451204]

Franaszczuk PJ, Bergey GK, Kaminski MJ. Analysis of mesial temporal seizure onset and propagation using the directed transfer function method. Electroencephalogr. Clin. Neurophysiol. 1994; 91(6): 413–427.

Fuchs M, Drenckhahn R, Wischmann H, Wagner M. An improved boundary element method for realistic volume-conductor modeling. IEEE Trans. Biomed. Eng. 1998; 45(8):980–997. [PubMed: 9691573]

Gevins A. High resolution EEG. Brain Topogr. 1993; 5(4):321–325. [PubMed: 8357701]

Grova C, Daunizeau J, Lina JM, Benar C, Benali H, Gotman J. Evaluation of EEG localization methods using realistic simulations of interictal spikes. Neuroimage. 2006; 29(3):734–753. [PubMed: 16271483]

NIH-PA Author Manuscript

NIH-PA Author Manuscript

NIH-PA Author Manuscript

Hamalainen M, Sarvas J. Realistic conductivity geometry model of the human head for interpretation of neuromagnetic data. IEEE Trans. Biomed. Eng. 1989; 36(2):165–171. [PubMed: 2917762]

Hämäläinen M, Hari R, Ilmoniemi RJ, Knuutila J, Lounasmaa OV. Magnetoencephalography–theory, instrumentation, and applications to noninvasive studies of the working human brain. Rev. Mod. Phys. 1993; 65(2):413–497.

Hansen PC. The discrete Picard condition for discrete ill-posed problems. BIT Numerical Math. 1990; 30(4):658–672.

He B, Musha T, Okamoto Y, Homma S, Nakajima Y, Sato T. Electric dipole tracing in the brain by means of the boundary element method and its accuracy. IEEE Trans. Biomed. Eng. 1987:406–414. [PubMed: 3610187]

Holmes MD, Tucker DM, Quiring JM, Hakimian S, Miller JW, Ojemann JG. Comparing noninvasive dense array and intracranial electroencephalography for localization of seizures. Neurosurgery. 2010; 66(2):354–362. [PubMed: 20087136]

Jung TP, Makeig S, Westerfield M, Townsend J, Courchesne E, Sejnowski TJ. Removal of eye activity artifacts from visual event-related potentials in normal and clinical subjects. Clin. Neurophysiol. 2000; 111(10):1745–1758. [PubMed: 11018488]

Knowlton RC, Elgavish RA, Al Bartolucci BO, Limdi N, Blount J, Burneo JG, Ver Hoef L, Paige L, Faught E, Kankirawatana P. Functional imaging: II. Prediction of epilepsy surgery outcome. Ann. Neurol. 2008; 64(1):35–41. [PubMed: 18570291]

Knowlton RC, Razdan SN, Limdi N, Elgavish RA, Killen J, Blount J, Burneo JG, Ver Hoef L, Paige L, Faught E. Effect of epilepsy magnetic source imaging on intracranial electrode placement. Ann. Neurol. 2009; 65(6):716–723. [PubMed: 19557860]

Koessler L, Benar C, Maillard L, Badier JM, Vignal JP, Bartolomei F, Chauvel P, Gavaret M. Source localization of ictal epileptic activity investigated by high resolution EEG and validated by SEEG. Neuroimage. 2010; 51(2):642–653. [PubMed: 20206700]

Kuzniecky R, Devinsky O. Surgery insight: surgical management of epilepsy. Nat. Clin. Pract. Neurol. 2007; 3(12):673–681. [PubMed: 18046440]

Lai Y, Van Drongelen W, Ding L, Hecox K, Towle V, Frim D, He B. Estimation of in vivo human brain-to-skull conductivity ratio from simultaneous extra-and intra-cranial electrical potential recordings. Clin. Neurophysiol. 2005; 116(2):456–465. [PubMed: 15661122]

Lantz G, Michel CM, Seeck M, Blanke O, Landis T, Rosén I. Frequency domain EEG source localization of ictal epileptiform activity in patients with partial complex epilepsy of temporal lobe origin. Clin. Neurophysiol. 1999; 110(1):176–184. [PubMed: 10348337]

Lantz G, Michel CM, Seeck M, Blanke O, Spinelli L, Thut G, Landis T, Rosén I. Space-oriented segmentation and 3-dimensional source reconstruction of ictal EEG patterns. Clin. Neurophysiol. 2001; 112(4):688–697. [PubMed: 11275543]

Lantz G, Grave de Peralta, R. Spinelli L, Seeck M, Michel C. Epileptic source localization with high density EEG: how many electrodes are needed? Clin. Neurophysiol. 2003; 114(1):63–69.

Laufs H, Duncan JS. Electroencephalography/functional MRI in human epilepsy: what it currently can and cannot do. Curr. Opin. Neurol. 2007; 20(4):417. [PubMed: 17620876]

Marsh ED, Peltzer B, Brown MW III, Wusthoff C, Storm PB Jr. Litt B, Porter BE. Interictal EEG spikes identify the region of electrographic seizure onset in some, but not all, pediatric epilepsy patients. Epilepsia. 2010; 51(4):592–601. [PubMed: 19780794]

Merlet I, Gotman J. Dipole modeling of scalp electroencephalogram epileptic discharges: correlation with intracerebral fields. Clin. Neurophysiol. 2001; 112(3):414–430. [PubMed: 11222962]

Michel CM, Lantz G, Spinelli L, de Peralta RG, Landis T, Seeck M. 128-channel EEG source imaging in epilepsy: clinical yield and localization precision. J. Clin. Neurophysiol. 2004; 21(2):71–83. [PubMed: 15284597]

Minassian BA, Otsubo H, Weiss S, Elliott I, Rutka JT, Snead OC. Magnetoencephalographic localization in pediatric epilepsy surgery: Comparison with invasive intracranial electroencephalography. Ann. Neurol. 1999; 46(4):627–633. [PubMed: 10514100]

Mosher JC, Lewis PS, Leahy RM. Multiple dipole modeling and localization from spatio-temporal MEG data. IEEE Trans. Biomed. Eng. 1992; 39(6):541–557. [PubMed: 1601435]

NIH-PA Author Manuscript

NIH-PA Author Manuscript

NIH-PA Author Manuscript

Nam H, Yim TG, Han SK, Oh JB, Lee SK. Independent component analysis of ictal EEG in medial temporal lobe epilepsy. Epilepsia. 2002; 43(2):160–164. [PubMed: 11903462]

Oostendorp TF, Delbeke J, Stegeman DF. The conductivity of the human skull: results of in vivo and in vitro measurements. Biomed. Eng. IEEE Trans. 2002; 47(11):1487–1492.

Palus M, Hoyer D. Detecting nonlinearity and phase synchronization with surrogate data. IEEE Eng. Med. Biol. Mag. 1998; 17(6):40–45. [PubMed: 9824760]

Pascual-Marqui R, Michel C, Lehmann D. Low resolution electromagnetic tomography: a new method for localizing electrical activity in the brain. Int. J. Psychophysiol. 1994; 18(1):49–65. [PubMed: 7876038]

Pataraia E, Simos P, Castillo E, Billingsley R, Sarkari S, Wheless J, Maggio V, Maggio W, Baumgartner J, Swank P. Does magnetoencephalography add to scalp video-EEG as a diagnostic tool in epilepsy surgery? Neurology. 2004; 62(6):943–948. [PubMed: 15037697]

Patel A, Alotaibi F, Blume WT, Mirsattari SM. Independent component analysis of subdurally recorded occipital seizures. Clin. Neurophysiol. 2008; 119(11):2437–2446. [PubMed: 18812266]

Plummer C, Harvey AS, Cook M. EEG source localization in focal epilepsy: where are we now? Epilepsia. 2008; 49(2):201–218. [PubMed: 17941844]

Ray A, Tao JX, Hawes-Ebersole SM, Ebersole JS. Localizing value of scalp EEG spikes: a simultaneous scalp and intracranial study. Clin. Neurophysiol. 2007; 118(1):69–79. [PubMed: 17126071]

Rosenow F, Luders H. Presurgical evaluation of epilepsy. Brain. 2001; 124(9):1683–1700. [PubMed: 11522572]

Schindler K, Leung H, Lehnertz K, Elger CE. How generalised are secondarily “generalised” tonic–clonic seizures? J. Neurol. Neurosurg. Psychiatry. 2007; 78(9):993–996. [PubMed: 17237141]

Spitzer AR, Cohen LG, Fabrikant J, Hallett M. A method for determining optimal interelectrode spacing for cerebral topographic mapping. Electroencephalogr. Clin. Neurophysiol. 1989; 72(4): 355–361. [PubMed: 2467802]

Srinivasan R, Nunez PL, Tucker DM, Silberstein RB, Cadusch PJ. Spatial sampling and filtering of EEG with spline Laplacians to estimate cortical potentials. Brain Topogr. 1996; 8(4):355–366. [PubMed: 8813415]

Stefan H, Hummel C, Scheler G, Genow A, Druschky K, Tilz C, Kaltenhauser M, Hopfengartner R, Buchfelder M, Romstock J. Magnetic brain source imaging of focal epileptic activity: a synopsis of 455 cases. Brain. 2003; 126(11):2396–2405. [PubMed: 12876149]

Theiler J, Eubank S, Longtin A, Galdrikian B, Doyne Farmer J. Testing for nonlinearity in time series: the method of surrogate data. Phys. D Nonlinear Phenomena. 1992; 58(1–4):77–94.

Towle VL, Yoon HA, Castelle M, Edgar JC, Biassou NM, Frim DM, Spire JP, Kohrman MH. ECoG gamma activity during a language task: differentiating expressive and receptive speech areas. Brain. 2008; 131(8):2013–2027. [PubMed: 18669510]

Tyvaert L, Hawco C, Kobayashi E, LeVan P, Dubeau F, Gotman J. Different structures involved during ictal and interictal epileptic activity in malformations of cortical development: an EEG-fMRI study. Brain. 2008; 131(8):2042–2060. [PubMed: 18669486]

Urrestarazu E, Iriarte J, Alegre M, Valencia M, Viteri C, Artieda J. Independent component analysis removing artifacts in ictal recordings. Epilepsia. 2004; 45(9):1071–1078. [PubMed: 15329072]

Vitikainen AM, Lioumis P, Paetau R, Salli E, Komssi S, Metsahonkala L, Paetau A, Kicic D, Blomstedt G, Valanne L, et al. Combined use of non-invasive techniques for improved functional localization for a selected group of epilepsy surgery candidates. Neuroimage. 2009; 45(2):342–348. [PubMed: 19159694]

Wheless J, Willmore L, Breier J, Kataki M, Smith J, King D, Meador K, Park Y, Loring D, Clifton G. A comparison of magnetoencephalography, MRI, and VEEG in patients evaluated for epilepsy surgery. Epilepsia. 1999; 40(7):931–941. [PubMed: 10403217]

Worrell GA, Lagerlund TD, Sharbrough FW, Brinkmann BH, Busacker NE, Cicora KM, O’Brien TJ. Localization of the epileptic focus by low-resolution electromagnetic tomography in patients with a lesion demonstrated by MRI. Brain Topogr. 2000; 12(4):273–282. [PubMed: 10912735]

Yang L, Liu Z, He B. EEG-fMRI reciprocal functional neuroimaging. Clin. Neurophysiol. 2010; 121(8):1240–1250. [PubMed: 20378397]

Zhang Y, van Drongelen W, He B. Estimation of in vivo human brain-to-skull conductivity ratio with the aid of intracranial electrical simulation. Appl. Phys. Lett. 2006; 89(1–3)

NIH-PA Author Manuscript

NIH-PA Author Manuscript

NIH-PA Author Manuscript

NIH-PA Author Manuscript

NIH-PA Author Manuscript

NIH-PA Author Manuscript

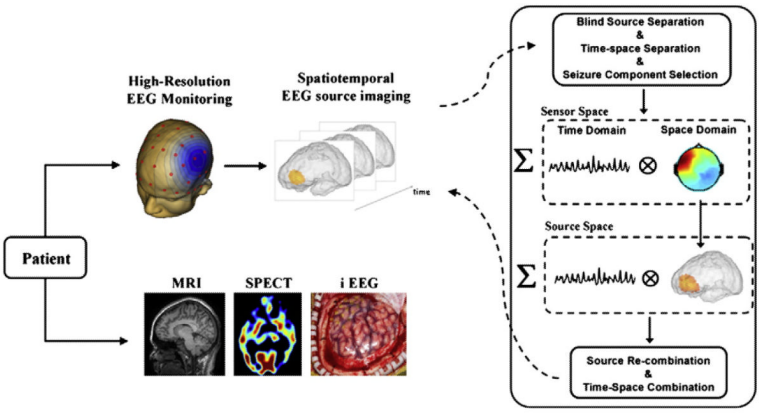

Fig. 1.

Schematic diagram depicting the non-invasive spatio-temporal seizure source imaging approach. We proposed prolonged 76-electrode video EEG monitoring. We further developed a spatiotemporal seizure imaging technique DSI based on a three-step procedure: (1) blind source separation and time–space separation in the sensor space; (2) source analysis performed separately in time and space domains; and (3) source re-combination and time–space re-combination in the source domain. The reconstructed seizure activities were compared to other clinical evidence, including surgically resected regions, iEEG recording, SPECT, and successful surgical outcome.

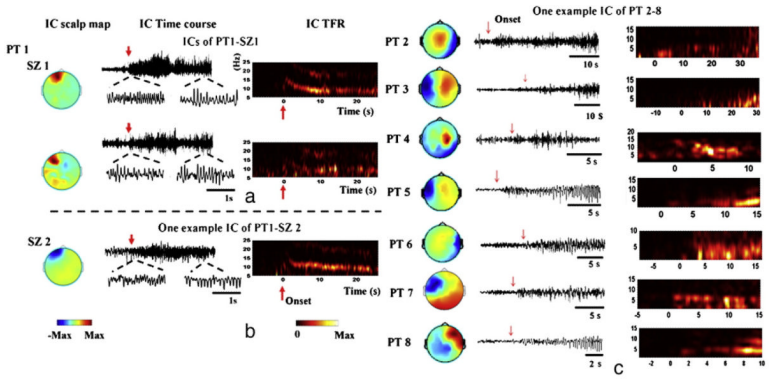

Fig. 2.

Examples of independent components identified in the 8 patients. (a) In one seizure recorded in patient 1, two independent components (ICs) were identified as seizure components. The IC time courses show ictal rhythms with increased frequency at seizure onset (red arrows) and decreased frequency in alpha band later. The IC TFRs further confirm the time–frequency evolution of ictal rhythms represented in the seizure components. The IC scalp maps indicate significant activation recorded in the left frontal electrodes with certain spread to temporal electrodes in the 2nd component. Other seizures recorded in the same patient showed similar spatial and temporal patterns of the independent components. (b) One example IC in seizure 2 of patient 1 showed similar spatial and temporal patterns. (c) Patients 2–8 presented with temporal lobe seizures. Multiple components were identified in each patient but only one example IC in each of the patients is shown here.

NIH-PA Author Manuscript NIH-PA Author Manuscript NIH-PA Author Manuscript

NIH-PA Author Manuscript

NIH-PA Author Manuscript

NIH-PA Author Manuscript

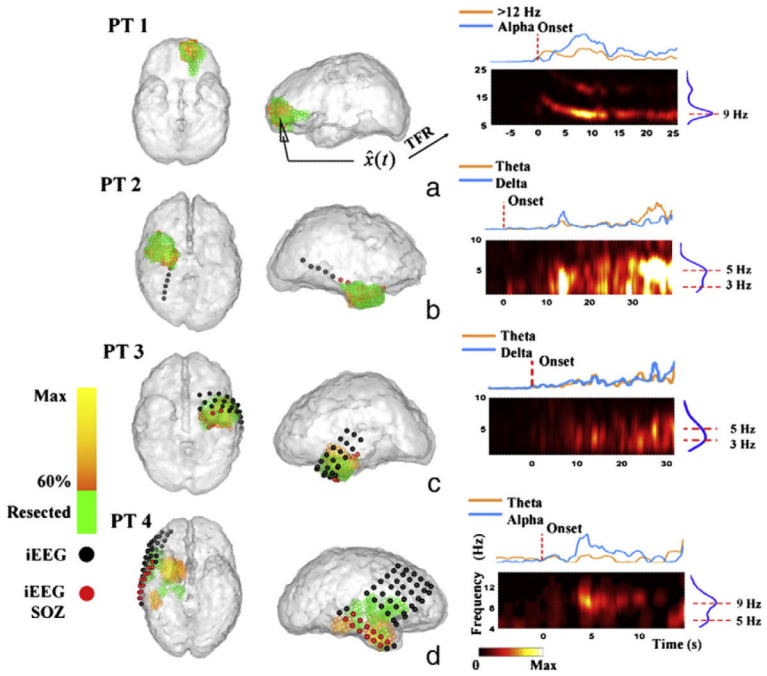

Fig. 3.

Seizure onset zones (SOZs) and the source TFRs estimated from a typical seizure in each of the patient 1–4. (a–d) The estimated SOZ (left and middle panels, 60% threshold, yellow to orange colorbar) is co-localized with surgically resected zones (shown in green) in patients 1–3, and SPECT foci (green) in patient 4. The TFR (right panels) shows the time– frequency evolution at the maximal estimated SOZ point. Intracranial electrodes were implanted in patient 2–4 (c–d, spherical dots). Epileptologists identified that seizures were initiated in (c) right temporal depth electrode (RTD) #1–3 (red spherical dots) in patient 2; (d) left anterior depth electrode (LAD) #1–3 (red spherical dots), left posterior depth electrode (LPD) #1–3 (red spherical dots), and left anterior temporal strip (LAT) #1–2 (red spherical dots) in patient 3; and (e) right inferior temporal strip (RIT) #2–7 (red spherical dots), and right mid-temporal strip (RMT) #2–7 (red spherical dots) in right temporal onset seizures in patient 4. Other grids/strips/depth electrodes not identified by epileptologists as SOZ were not shown in the figures.

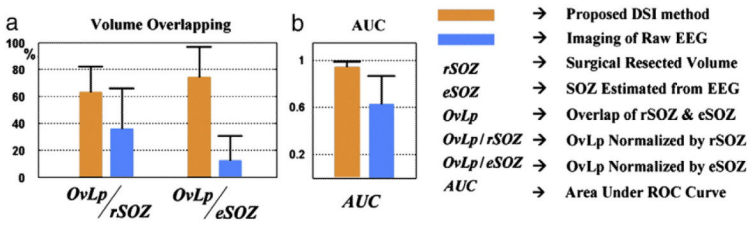

Fig. 4.

Performance of the SOZ localization using the DSI method (orange bar) in comparison with the SOZ localization by applying source imaging directly on raw EEG instant by instant (blue bar). (a) The mean and standard deviation of the volume overlapping between the estimated SOZs (60% threshold) and surgically resected regions/SPECT foci in the 17 seizures. (b) Mean and standard deviation of the AUC index derived from ROC analysis. A higher AUC index in the range of [0, 1] implies greater localization accuracy.

NIH-PA Author Manuscript
NIH-PA Author Manuscript
NIH-PA Author Manuscript

NIH-PA Author Manuscript

NIH-PA Author Manuscript

NIH-PA Author Manuscript

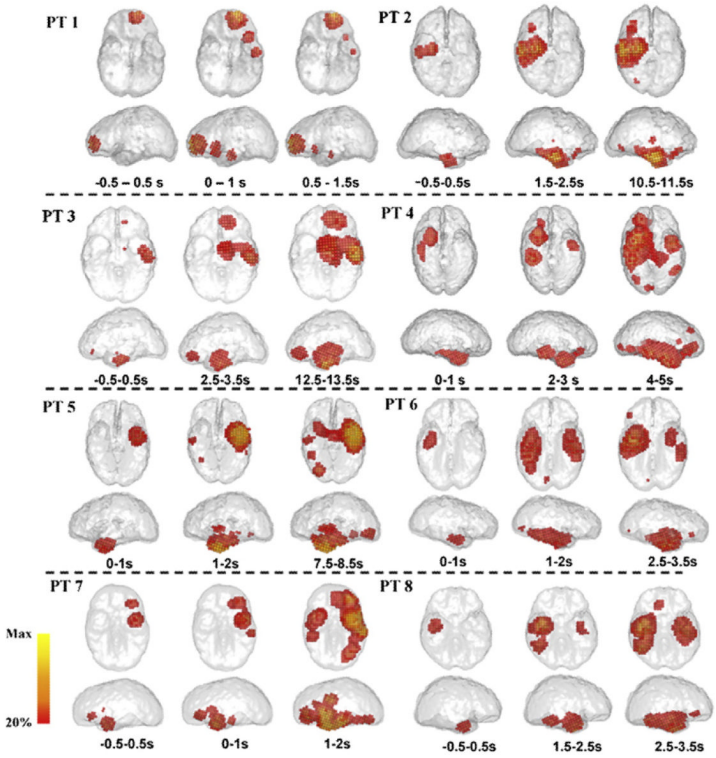

Fig. 5.

Time-varying source power distribution in one seizure of each patient. We displayed the spectral power distribution within the predominant frequency band of ictal rhythm calculated using 1-s sliding window.

NIH-PA Author Manuscript

NIH-PA Author Manuscript

NIH-PA Author Manuscript

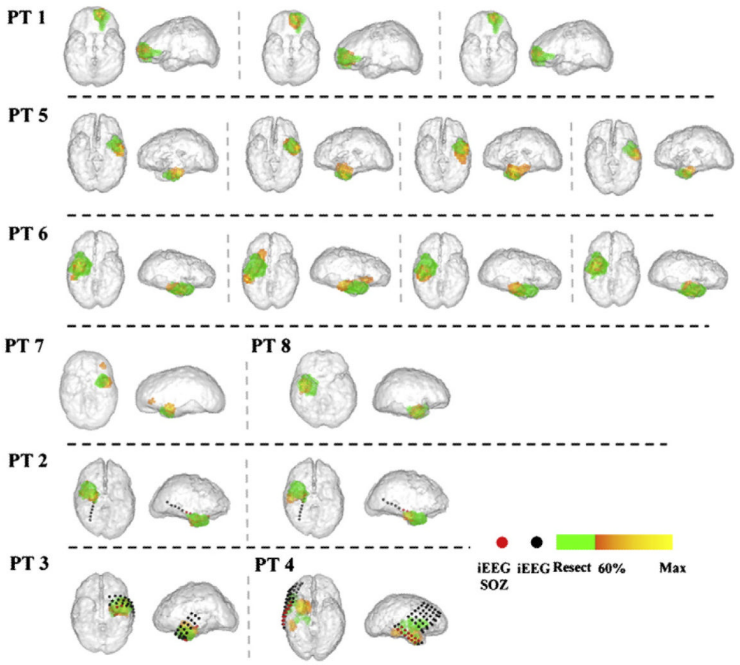

Fig. 6.

SOZs reconstructed from all the 17 seizures in the 8 patients. The estimated SOZs (60% threshold, yellow to orange color bar) were displayed with surgical resected zones or SPECT foci (green) and SOZ identified using iEEG (red dots).

NIH-PA Author Manuscript NIH-PA Author Manuscript NIH-PA Author Manuscript

Neuroimage. Author manuscript; available in PMC 2012 June 15.

Table 1

Patient information including inter-ictal EEG, semiology, etiology, MRI, intracranial SOZ and surgery outcomes.

Pt	Interictal EEG	Semiology	Etiology	MRI	Intracranial SOZ	Surgery and pathology
Pt 1 sex: F	Right and left frontal and frontopolar spikes	Left hand nose wiping, and oral automatisms	Cryptogenic	Left frontal polar encephalomalcia	N/A	Left frontal cortectomy Outcome: ILAE-1 Pathology: sub cortical and subpial gliosis
Pt 2 sex: M	Right and left temporal spikes	Swallowing and oral automatisms; non-forced head turning to left	Cryptogenic	Normal	RTD 1–3	Right ATL Outcome: ILAE-1 Pathology: right temporal subpial gliosis HC: severe gliosis
Pt 3 sex: F	Independent right and left temporal spikes	Right hand automatisms, oral automatisms, ictal scream, and hypermotor activity	Cryptogenic	Normal	LAT #1, 2; LAD #1–3 LPD #1–3	Left ATL Outcome: ILAE-1 Pathology: gliosis, subpia, subcortical, entorhinal cortex
Pt 4 sex: M	Right frontal and temporal spikes	Forced head turn to the right and an ictal cry	Cryptogenic, but likely related to post-surgical encephalomalcia	Right frontal encephalomalacia 2nd to remote history of craniopharyngioma	RIT amd RMT #2–7; spread to the inferior contacts of the RG; independent L. temporal seizures	History of surgery for craniopharyngioma
Pt 5 sex: M	Left temporal sharp waves and left TIRDA	Behavioral arrest, oral automatisms, and right arm posturing	MTS	Left HC atrophy and T2 signal	N/A	Left ATL Outcome: ILAE-1 Pathology: MTS
Pt 6 sex: F	Right temporal spikes	Behavioral arrest, oral automatisms, and right arm posturing	Cryptogenic	Mild generalized cerebellar atrophy	N/A	Right ATL Outcome: ILAE-2 Pathology: severe subpial gliosis consistent with chronic seizure disorder
Pt 7 sex: M	Left temporal spikes and TIRDA	Behavior arrest followed by oral automatisms	Cryptogenic	Focal mass anterior left temporal lobe	N/A	Excision of left temporal lobe lesion Outcome: ILAE-1 Pathology: gliosis
Pt 8 sex: F	Right temporal spikes	Sense of impending doom, oral automatisms	MTS	Right HC atrophy	N/A	Right: ATL Outcome: ILAE-1 Pathology: MTS

Hippocampus (HC), mesial temporal sclerosis (MTS), ILAE (International League against epilepsy), right and left temporal depth (RTD and LTD), right middle temporal (RMT), right inferior temporal (RIT), left temporal grid (LTG), left anterior temporal (LAT), left anterior temporal depth (LAD), left posterior temporal depth (LPD), anterior temporal lobectomy (ATL), temporal intermittent rhythmic delta activity (TIRDA).